COMMUNICATION

Check for updates

B2-structured indium–platinum group metal high-entropy intermetallic nanoparticles†

Masashi Nakamura,[a] Dongshuang Wu,*[a] Megumi Mukoyoshi, [ID][a] Kohei Kusada, [ID][ab]
Takaaki Toriyama,[c] Tomokazu Yamamoto,[c] Syo Matsumura,[d] Yasukazu Murakami,[ce]
Shogo Kawaguchi, [ID][f] Yoshiki Kubota[g] and Hiroshi Kitagawa [ID]*[a]

We first report the synthesis of B2-structured indium–platinum group metal high-entropy intermetallic nanoparticles (In–PGM HEI NPs). The synthesis was achieved by a wet-chemistry method and subsequent heat treatment. The crystal structure of these NPs is unique in the coexistence of completely orderly arranged indium and disorderly arranged PGMs.

High-entropy alloys (HEAs) are defined as multi-element alloys stabilised by a configurational entropy higher than $1.5R$ arising from random distribution of the elements in the crystal structures.[1] Their huge compositional space expands the materials library significantly.[2,3] The HEA nanoparticles (NPs) have been extensively studied as prospective nanomaterials, distinct from conventional alloy NPs.[4] In particular, the platinum group metal (PGM)-based HEA NPs are attracting attention because of their excellent catalytic performance.[5–8] To date, a variety of HEA NPs composed of a variety of elemental combinations have been reported, but most of these possess a face-centred cubic (fcc) structure.[4–8] Crystal structures that are not fcc, such as hexagonal close packing (hcp) and body-centred cubic (bcc), have rarely been reported for PGM-based HEA NPs.

[a] *Division of Chemistry, Graduate School of Science, Kyoto University, Kitashirakawa-Oiwakecho, Sakyo-ku, Kyoto 606-8502, Japan. E-mail: dongshuang.wu@ntu.edu.sg, kitagawa@kuchem.kyoto-u.ac.jp*

[b] *The HAKUBI Center for Advanced Research, Kyoto University, Kitashirakawa-Oiwakecho, Sakyo-ku, Kyoto 606-8502, Japan*

[c] *The Ultramicroscopy Research Center, Kyushu University, 744 Motooka, Nishi-ku, Fukuoka 819-0395, Japan*

[d] *National Institute of Technology, Kurume College, 1-1-1 Komorino, Kurume, Fukuoka 830-8555, Japan*

[e] *Department of Applied Quantum Physics and Nuclear Engineering, Graduate School of Engineering, Kyushu University, 744 Motooka, Nishi-ku, Fukuoka 819-0395, Japan*

[f] *Japan Synchrotron Radiation Research Institute (JASRI), SPring-8, 1-1-1 Kouto, Sayo-cho, Sayo-gun, Hyogo 679-5198, Japan*

[g] *Department of Physics, Graduate School of Science, Osaka Metropolitan University, 1-1 Gakuen-cho, Naka-ku, Sakai, Osaka 599-8531, Japan*

† Electronic supplementary information (ESI) available: Experimental details, X-ray spectroscopic data and electron microscopic images. See DOI: https://doi.org/10.1039/d3cc02266h
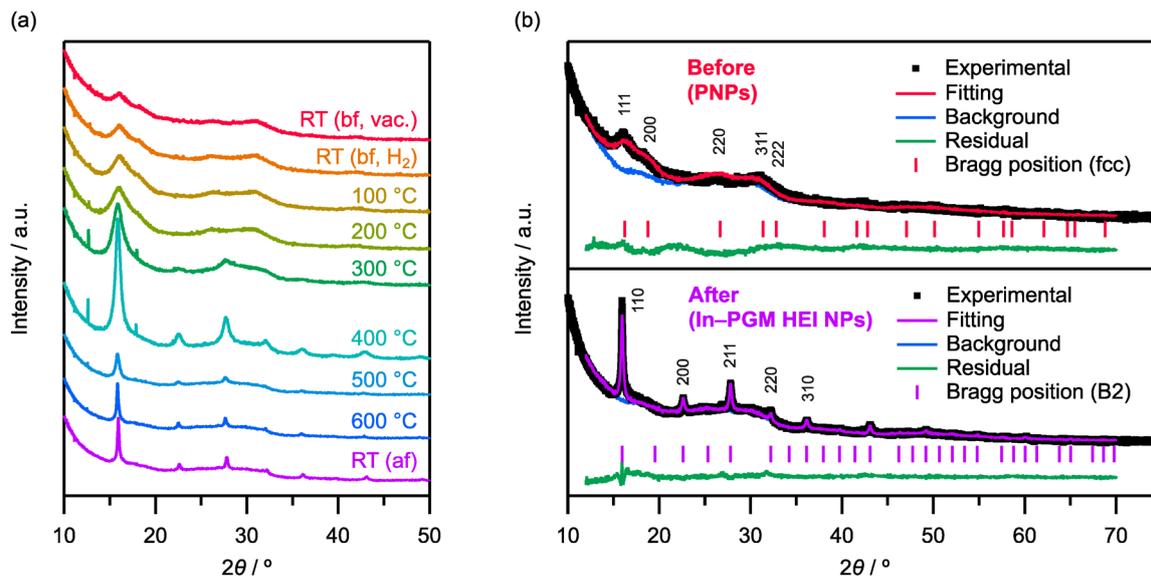
To engineer the atomic arrangement of PGMs in HEA NPs, we focused on intermetallic phases where the different elements are orderly arranged in different crystallographic sites. Quite recently, high-entropy intermetallic (HEI) NPs have emerged as a new class of high-entropy nanomaterials.[9–12] The HEI crystal structures have more than one non-equivalent site, and the random occupation of several elements in at least one site results in the high configurational entropy. In principle, electronically and geometrically similar elements tend to form disordered solid solutions, and dissimilar elements lead to ordered intermetallic compounds with crystal lattices that differ from their end components.[13–15] Our study targeted five PGMs (Ru, Rh, Pd, Ir and Pt), all of which have a similar nature, aiming to mix them randomly at the same crystallographic site. Then, indium was selected to modulate the arrangement of PGMs because it has distinctively smaller electronegativity and a larger atomic radius than PGMs.[16,17]

Here, we first synthesised the B2-structured HEI NPs composed of indium and PGMs (In–PGM HEI NPs) in two steps. First, precursor NPs (PNPs) were prepared by reducing the precursors of all the constitutional metal elements using a wet-chemistry method. Then, In–PGM HEI NPs were obtained by heat treatment of the PNPs. The formation of the HEI NPs at a mild condition, 300 °C, was verified by synchrotron *in situ* powder X-ray diffraction (PXRD). Atomic-resolution structure analysis with scanning-transmission electron microscopy (STEM) revealed that indium and the PGMs occupied different sublattices in a B2 structure, namely, an ordered bcc structure where the body centre site and the corner site is no longer equivalent.

The PNPs were synthesised by the following procedure. First, triethylene glycol (TEG) solutions of metal precursors and sodium borohydride (NaBH₄), a reducing agent, were separately prepared. Among the metal precursors, the indium molar fraction was 50%, and the rest was equally divided between five PGMs. These two solutions were injected into a TEG solution of polyvinylpyrrolidone (PVP), a protecting agent, that was preliminarily heated up to 200 °C under Ar atmosphere.

Fig. 1 (a) *In situ* synchrotron PXRD patterns in the range of 10°−50°. The incident X-ray wavelength was 0.630407(1) Å. (b) Structure analysis of the NPs before and after heating. The fitting was performed by Rietveld refinement in the range of 12°−70°. The estimated structural parameters are shown in Table 1.

Table 1 The fitting statistics and estimated structures corresponding to the Rietveld analysis shown in Fig. 1b

		wR/%	GOF	Space group	Lattice constant/Å	Crystallite size/nm
Before	PNPs	3.39	2.54	$Fm\bar{3}m$	3.865(4)	1.28(2)
After	In–PGM HEI NPs	3.45	1.83	$Pm\bar{3}m$	3.2121(2)	12.5(1)

Considering the decomposition of $NaBH_4$, both solutions were concurrently injected, but to ensure sufficient reduction, the $NaBH_4$ solution was continuously injected even before and after the injection of the precursor solution. Immediately after the injection was completed, the solution was rapidly cooled down to room temperature (RT) in an ice–water bath. Finally, the target NPs were collected by centrifugation. The PNP composition was consistent with the nominal ratios confirmed by X-ray fluorescence spectroscopy (XRF) (Fig. S1, ESI†). Transmission electron microscopy (TEM) images showed that the PNPs were covered by blurred layers (Fig. S2, ESI†).

The PNPs were placed into a glass capillary to trace the structural change *in situ* by synchrotron PXRD at SPring-8 beamline BL02B2.[18,19] The heat treatment was conducted under H_2 atmosphere at 1 atm from RT to 600 °C. The PXRD profiles were acquired under vacuum before and after heating in H_2. The changes in the PXRD profiles are shown in Fig. 1a. The peaks become slightly sharper with increasing temperature from RT to under 200 °C. Then, new peaks appear at 300 °C and sharpen with increasing temperature. The temperature of 300 °C is higher than the TEG boiling point, the wet-chemically achievable temperature limit, but lower than the synthesis temperature of HEI NPs in prior studies (typically more than 600 °C was applied).[9–12] The diffraction patterns before and after heating were analysed by Rietveld refinement using GSAS-II software[20] (Fig. 1b and Table 1). The sample has small-sized fcc-structured NPs before heating, but after heating, these

turned into larger-sized B2-structured NPs. In detail, the lattice parameter before change was 3.865(4) Å, slightly larger than the reported value of fcc-structured PGM HEA NPs,[5] indicating indium incorporation into the fcc lattice. However, it is supposed that not all the indium was incorporated in the fcc lattice based on Vegard's law,[21] as anticipated from the redox potential and crystal structure of indium. The extra indium would be in the blurred layers found in the TEM images, assumingly ascribed to amorphous oxide clusters, which are difficult to see in the PXRD patterns. After the change, the lattice parameter of the B2 phase was 3.2121(2) Å and the bond distance between the nearest neighbours increased compared with the as-synthesised fcc-structured PNPs, indicating further incorporation of atoms with larger atomic radius, namely indium, into the alloy by the treatment. The results above support that B2 structured In–PGM HEI NPs can be synthesised by heating PNPs at more than 300 °C.

The crystal structures were further examined by high-angle annular dark-field scanning-transmission electron microscopy (HAADF-STEM). To make it easier to visualise NPs avoiding spatial overlap in images, the PNPs were loaded on amorphous carbon and heated at 350 °C under 1 atm of H_2 for 20 min. Comparing the PXRD patterns before and after the heating, the structural change in the *in situ* test could well be reproduced (Fig. S4, ESI†). In STEM images, 2 nm size particles were found in the fcc structure before heating (Fig. S5, ESI†). The lattice parameter estimated from lattice patterns was 3.9 Å, roughly
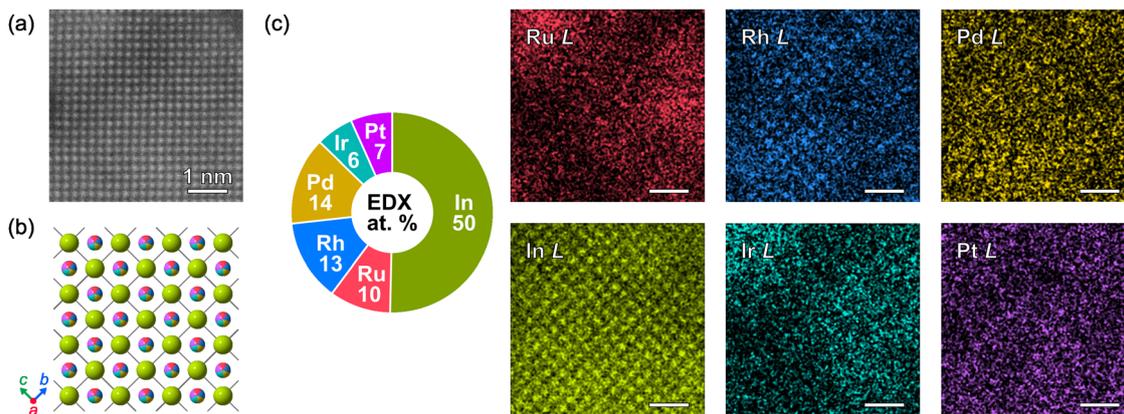
Fig. 2 (a) Atomic-resolution HAADF-STEM image of In–PGM HEI NPs/C viewed along the [100] axis. (b) Expected view of B2-structured In–PGM HEI NPs along the same axis as (a). Green atoms are indium and colourful atoms are any one of the PGMs. (c) Compositional information obtained in EDX analysis corresponding to the region in (a). The pie chart in the top left shows compositions of the whole region and the right six figures show elemental maps based on characteristic X-rays of each constitutional element. The scale bars in the EDX maps represent 1 nm.

equivalent to PXRD results. Most of the particles were covered with clusters without lattice patterns, which is assumingly ascribed to amorphous metal oxide mainly composed of indium, as noted above. After heating, NPs larger than 5 nm in size were found in a B2 structure whose lattice parameter was about 3.2 Å (Fig. S6, ESI†). These particles were often found in aggregations with the remaining oxide cluster, suggesting that HEI NPs grew by the take-up of indium atoms in the oxide clusters.

The atomic number of indium is approximately comparable to the averaged atomic number of PGMs. Because both PXRD and HAADF-STEM discern the elemental species based on scattering factors monotonically related to the atomic number, it was difficult to see superlattice reflections in the PXRD patterns or to distinguish different sublattices by Z-contrast in the HAADF-STEM images. Thus, the results above were not sufficient to provide evidence of the ordered atomic arrangement. Atomic-resolution energy dispersive X-ray (EDX) analysis was performed to verify the ordering (Fig. 2). The region of interest is shown in Fig. 2a and the B2-structured crystal is viewed along the [100] axis. If the lattice is ordered, the different sublattices

can be distinguished in this view (Fig. 2b). In fact, the experimental EDX map of In L line clearly shows that indium occupies one of the sublattices (Fig. 2c and Fig. S7 in ESI†). Although the individual EDX maps of PGMs are not sufficiently clear to support the ordering because of their lower molar contents, the composition of the whole image showed a molar ratio of 1:1 of indium to PGMs, indicating that the PGMs occupy the sublattice other than indium. Also, the EDX line profile showed alternating peaks of characteristic X-ray net counts from indium and all the PGMs (Fig. 3). These results strongly support the formation of the B2-structured HEI in which one sublattice is occupied solely by indium and the other is randomly occupied by five PGMs, formulated as In(Ir,Rh,Ru,Pd,Pt). The configurational entropy was evaluated according to the concept of the entropy metric (EM) proposed by Dippo and Vecchio;[22] the EM calculated based on the compositions was $1.55R$, exceeding $1.5R$ and therefore meeting the definition of a high-entropy material.

The formation of the structure is assumed to be affected by the electronegativity and atomic radii of the constitutional
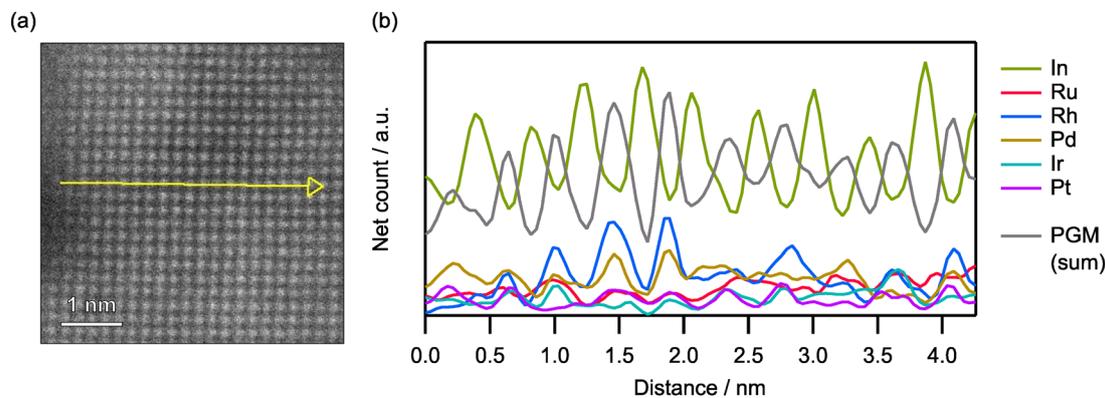

Fig. 3 Atomic-resolution EDX line analysis of In–PGM HEI NPs/C. (a) The HAADF-STEM image of the target B2-structured HEI NPs viewed along the [100] axis. The yellow arrow shows the region of interest. (b) The line profiles of the characteristic X-ray net counts from each constitutional element and the chem sum of PGMs.

elements. PGMs are neighbours in the periodic table, and thus have similar electronic and geometric features.[16,17] As a result, they are randomly distributed in the same sublattice. By contrast, the indium atom presents distinctively different electronegativity and atomic radius than do PGMs[16,17] because valence electrons in indium experience smaller effective nuclear charge than those of PGMs. Consequently, indium is located in the other sublattice than PGMs. The stabilisation of the B2 structure among a variety of possible intermetallic phases can be associated with the B2-structured binary or ternary intermetallic NPs, such as InPd,[23,24] InRh[25] and In(Pd,Pt).[26] Finally, we want to emphasise the uniqueness of the structure of the In–PGM HEI NPs. Even in the single-phase alloy, PGMs disorderly occupy half of the sites while indium occupies the other half in a completely orderly manner. The coexistence of ordered and disordered metal elements could be a clue for developing distinctive properties or functionalities in alloy nanomaterials, such as enhancement in selectivity as a catalyst.

In conclusion, we reported the first synthesis of B2-structured HEI NPs composed of indium and PGMs with totally different electronegativity and atomic radii. In the NPs, the PGMs occupy one of the sublattices in a B2 structure, not an fcc structure. The synthesis was achieved by the heat treatment of the wet-chemically prepared precursor NPs under the relatively mild condition. The atomic number similarity of the constituent elements did not allow observation of the ordering unique to the intermetallic phase; nevertheless, we confirmed it by atomic-resolution EDX analysis. Our results could pave the way for developing a new class of nanoalloys characterised by both aspects of order and disorder.

Conflicts of interest

There are no conflicts to declare.

Notes and references

1 J.-W. Yeh, S.-K. Chen, S.-J. Lin, J.-Y. Gan, T.-S. Chin, T.-T. Shun, C.-H. Tsau and S.-Y. Chang, *Adv. Eng. Mater.*, 2004, **6**, 299–303.
2 B. S. Murty, J.-W. Yeh and S. Ranganathan, *High-Entropy Alloys*, Butterworth-Heinemann, Oxford, 2014.
3 D. B. Miracle and O. N. Senkov, *Acta Mater.*, 2017, **122**, 448–511.
4 Y. Yao, Z. Huang, P. Xie, S. D. Lacey, R. J. Jacob, H. Xie, F. Chen, A. Nie, T. Pu, M. Rehwoldt, D. Yu, M. R. Zachariah, C. Wang, R. Shahbazian-Yassar, J. Li and L. Hu, *Science*, 2018, **359**, 1489–1494.
5 D. Wu, K. Kusada, T. Yamamoto, T. Toriyama, S. Matsumura, I. Gueye, O. Seo, J. Kim, S. Hiroi, O. Sakata, S. Kawaguchi, Y. Kubota and H. Kitagawa, *Chem. Sci.*, 2020, **11**, 12731–12736.
6 D. Wu, K. Kusada, T. Yamamoto, T. Toriyama, S. Matsumura, S. Kawaguchi, Y. Kubota and H. Kitagawa, *J. Am. Chem. Soc.*, 2020, **142**, 13833–13838.
7 D. Wu, K. Kusada, Y. Nanba, M. Koyama, T. Yamamoto, T. Toriyama, S. Matsumura, O. Seo, I. Gueye, J. Kim, L. S. Rosantha Kumara, O. Sakata, S. Kawaguchi, Y. Kubota and H. Kitagawa, *J. Am. Chem. Soc.*, 2022, **144**, 3365–3369.
8 Y. Sun and S. Dai, *Sci. Adv.*, 2021, **7**, eabg1600.
9 J. Ma, F. Xing, Y. Nakaya, K. Shimizu and S. Furukawa, *Angew. Chem., Int. Ed.*, 2022, **61**, e202200889.
10 F. Xing, J. Ma, K. Shimizu and S. Furukawa, *Nat. Commun.*, 2022, **13**, 5065.
11 M. Cui, C. Yang, S. Hwang, M. Yang, S. Overa, Q. Dong, Y. Yao, A. H. Brozena, D. A. Cullen, M. Chi, T. F. Blum, D. Morris, Z. Finfrock, X. Wang, P. Zhang, V. G. Goncharov, X. Guo, J. Luo, Y. Mo, F. Jiao and L. Hu, *Sci. Adv.*, 2022, **8**, eabm4322.
12 D. Wang, Z. Chen, Y. Wu, Y. Huang, L. Tao, J. Chen, C. Dong, C. V. Singh and S. Wang, *SmartMat*, 2023, **4**, e1117.
13 W. Hume-Rothery and G. V. Raynor, *The Structure of Metals and Alloys*, The Institute of Metals, Belgrave Square, London, 1962.
14 S. Mizushima and I. Ichishima, *Proc. Jpn. Acad.*, 1967, **43**, 369–374.
15 H. Wang, Q.-F. He and Y. Yang, *Rare Met.*, 2022, **41**, 1989–2001.
16 L. Pauling, *The Nature of the Chemical Bond*, Cornell Univ Press, Ithaca, New York, 3rd edn, 1960.
17 D. R. Lide, *CRC Handbook of Chemistry and Physics*, CRC Press, Boca Raton, Florida, 85th edn, 2004.
18 S. Kawaguchi, M. Takemoto, K. Osaka, E. Nishibori, C. Moriyoshi, Y. Kubota, Y. Kuroiwa and K. Sugimoto, *Rev. Sci. Instrum.*, 2017, **88**, 085111.
19 S. Kawaguchi, M. Takemoto, H. Tanaka, S. Hiraide, K. Sugimoto and Y. Kubota, *J. Synchrotron Radiat.*, 2020, **27**, 616–624.
20 B. H. Toby and R. B. Von Dreele, *J. Appl. Crystallogr.*, 2013, **46**, 544–549.
21 A. R. Denton and N. W. Ashcroft, *Phys. Rev. A*, 1991, **43**, 3161–3164.
22 O. F. Dippo and K. S. Vecchio, *Scr. Mater.*, 2021, **201**, 113974.
23 T. Komatsu, *Appl. Catal., A*, 2003, **251**, 315–326.
24 A. García-Trenco, A. Regoutz, E. R. White, D. J. Payne, M. S. P. Shaffer and C. K. Williams, *Appl. Catal., B*, 2018, **220**, 9–18.
25 S. Furukawa, A. Yokoyama and T. Komatsu, *ACS Catal.*, 2014, **4**, 3581–3585.
26 J. Jeon, H. Ham, F. Xing, Y. Nakaya, K. Shimizu and S. Furukawa, *ACS Catal.*, 2020, **10**, 11380–11384.